JOM, Vol. 76, No. 6, 2024
https://doi.org/10.1007/s11837-024-06502-9

Uncertainty Analysis for Ferromagnetic-Paramagnetic Phase Transition Behavior of Magnetic Materials

ZEKERIYA ENDER EGER[1,2] and PINAR ACAR[1,3]

1.—Department of Mechanical Engineering, Virginia Tech, 635 Prices Fork Rd, Blacksburg, VA 24061, USA. 2.—e-mail: endereger@vt.edu. 3.—e-mail: pacar@vt.edu

This study aims to model the phase transition of ferromagnetic materials using two- (2D) and three-dimensional (3D) Ising models, incorporating long-range magnetic spin-to-spin interactions and the influence of an external magnetic field. The 2D Ising model is investigated mainly for a 4×4 domain, while its extension to larger domains is also explored. For the 3D Ising model, the selection of representative volume element is discussed in terms of free energy. An uncertainty quantification formulation is integrated into the Ising model to capture the uncertainties related to the external magnetic field and evaluate their effects on the phase transition from a ferromagnetic to a paramagnetic state. Despite the common use and known effectiveness of the Ising model, there is still no universally accepted exact solution for the 3D domains, making it an ongoing research focus. The research also acknowledges the complexities and limitations arising from experimental methods, despite the insights they provide on the microscopic dynamics of ferromagnetic materials during phase transitions.

INTRODUCTION

Ferromagnetic materials are integral to many branches of engineering, primarily in transportation and energy sectors, given their unique magnetic properties.[1–4] However, these materials have a tendency to lose their magnetism at elevated temperatures because of an irreversible phase transition, a phenomenon that compromises their functionality in various systems. In the ferromagnetic state, the system's atomic spins are aligned because of their robust interactions with one another. This alignment produces a powerful magnetic field, contributing to the material's usefulness in energy and transportation applications. Nevertheless, this advantage becomes a liability when the material is exposed to high temperatures as the ferromagnetic materials transit to a paramagnetic state. During this phase transition, the atomic spins' interaction strength diminishes, resulting in a state where the spins are randomly oriented rather than aligned.[5] In this state, the material can only be magnetized temporarily, and that too when an external magnetic field is present.[6] The susceptibility to external magnetic fields forms an important component of the physics behind the phase transition, a concept thoroughly addressed by the Ising model.

The Ising model, a vital tool in statistical mechanics, elucidates this phenomenon. It provides an explanation for the spin interactions and predicts the system's state based on the principle of minimum free energy. In particular, the Ising model defines magnetization as a parameter varying between –1 and 1 for ferromagnetic materials (where spins are aligned in different directions) and 0 for a paramagnetic state. These magnetization values serve as critical indicators of the material's phase.[7] When it comes to the Ising model, solutions developed for different dimensions have been a point of focus. For a one-dimensional (1D) system, a clear and concise solution exists.[8] The simplicity of the 1D case allows for an exact analytical solution, leading to a detailed understanding of spin interactions in such systems. The two-dimensional (2D) Ising model, however, is more complicated. Simplifications are necessary to find analytical solutions for this case. These include the

(Received June 9, 2023; accepted March 8, 2024; published online April 15, 2024)

consideration of an infinitely-sized lattice and the disregard for long-range interactions. In 1944, Lars Onsager solved the 2D Ising model without an external magnetic field, a landmark achievement in the field of statistical mechanics.[9] The situation becomes more complex when the Ising model is extended to three dimensions, 3D). Despite considerable efforts, no universally accepted solution for the 3D Ising model has been found so far, which continues to be an active area of ongoing research. Some approximate solutions and computer simulations offer insights, but the precise nature of phase transitions in three dimensions remains elusive.[10–16] Moreover, uncertainties related to the external magnetic field and the temperature must be investigated as they may affect the phase transition region while their effects have not been addressed in the literature to the best of the authors' knowledge.

Besides the theoretical Ising model, other models and experimental methods are employed to explore the phase transition phenomena. Researchers have employed sophisticated techniques like neutron scattering, magnetometry, and electron microscopy to probe the microscopic structure and dynamics of ferromagnetic materials during the phase transition.[17–19] These techniques have helped identify key features of the transition, such as changes in spin alignment and the formation of magnetic domains. Despite these advancements, experimental studies often face challenges related to specificity and generalization. Observations and results are typically specific to the material under study, making it difficult to extrapolate the findings to other materials.[20–22] Additionally, experimental data often require theoretical models for interpretation, leading to some dependence on models like the Ising model. While these approaches can provide valuable insights, they often face limitations in generalizability, with experiments often tailored to specific materials. Therefore, the research for a more comprehensive understanding of phase transitions in ferromagnetic materials continues, an endeavor underlined by the fundamental role these materials play in various applications.

In this study, our focus lies in formulating both two-dimensional (2D) and three-dimensional (3D) Ising models. These models are designed to consider the impact of long-range magnetic spin-spin interactions, especially in the presence of an external magnetic field. A statistical model is used to model the long-range interactions based on the distance and temperature.[23] Following this, we introduce an uncertainty quantification (UQ) framework into the Ising models, aiming to assess the uncertainties related to the external magnetic field and temperature.[24,25] We also evaluate the effects of these uncertainties on the phase transition behavior, when moving from a ferromagnetic to a paramagnetic state. Our numerical methodology is verified using exhaustive search solutions. The structure of this article unfolds as such: The subsequent section, "Mathematical Modeling" section, delves into the formulation of the 2D and 3D Ising models. The subsequent findings and discussions, including extended mean field solutions and the analysis of uncertainty, are documented in "Results and Discussions" section. "Conclusion" section offers a summary of the article and hints at potential future research directions to be pursued.

MATHEMATICAL MODELING

A high-fidelity numerical model is developed to investigate the boundaries of the phase transition region. The region is defined based on the variation of the external magnetic field and temperature as shown in Fig. 1. The spins in the structure of any material are bound to be stochastic, meaning that they tend to point in a different direction continuously. These spins can either be +1 or –1 for the Ising problem.

Two-dimensional Ising Model

The energy function for the Ising model, which takes into account the impacts of an external magnetic field, is defined as:[16]

$$H = -\omega_j \Sigma_{<i,j>} \sigma_i \sigma_j - h \Sigma_i \sigma_i \tag{1}$$

In this equation, h signifies the non-dimensional external magnetic field parameter, σ symbolizes the spin parameter, and $\sigma_i \sigma_j$ stands for the interactions between the spins denoted by indices i and j. In this context, indices i and j also incorporate the long-range spins. Introduced in Eq. 1, the ω_j parameter represents the weight parameter that indicates the strength of spin-to-spin interactions, relevant to the corresponding level of neighboring information incorporated into the Hamiltonian energy equation. The state of a particular spin is influenced by a combination of nearest-neighbor interactions and long-range order interactions. The interaction strength between the spins regardless of their distances regarding each other at low temperatures is observed to be almost equal. However, increasing the temperature causes a shift in the distribution, and long-range neighbors start having less effect compared to nearby neighbors. After the phase transition occurs, this trend continues, and the strength of any spin rather than the nearest spins is completely diminished. Even though the strength is not explicitly defined in the literature for all different temperature values, the relation is explained with the correlation function for three main cases: $T > T_c, T < T_c$, and $T = T_c$. T_c is the Curie temperature, the point where the phase transition occurs. For these cases, there are models attempting to explain the relation. Using the main idea and these models, a statistical model is created. The model reflects the behavior of the correlation function in Fig. 2, which is based on a Gaussian distribution. In

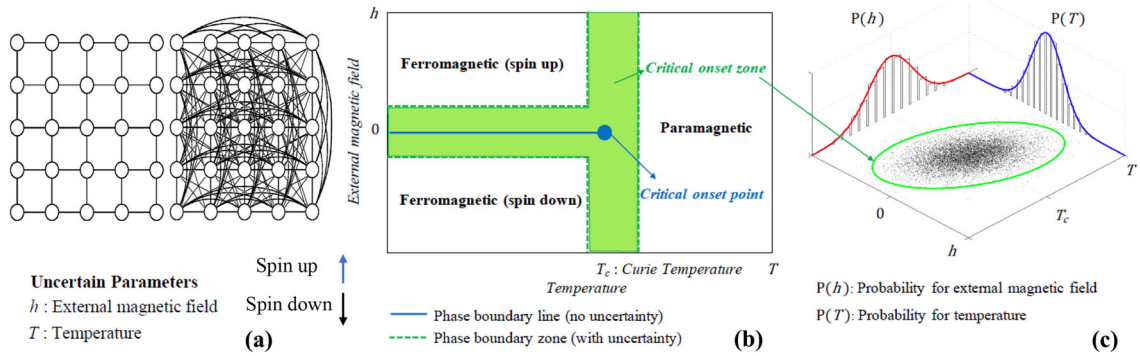

Fig. 1. (a) The 2D lattice, where each circle represents a node which can hold two states: spin-up (+ 1) and spin-down (− 1), controlled by the external magnetic fields and temperature. Bonds are used to connect neighbor nodes. (b) Considering the uncertainties in external fields and temperature, the phase transition occurs at a critical 'zone.' (c) The likelihood of the phase transition in this zone can be computed with a joint probability representation of the uncertain parameters.

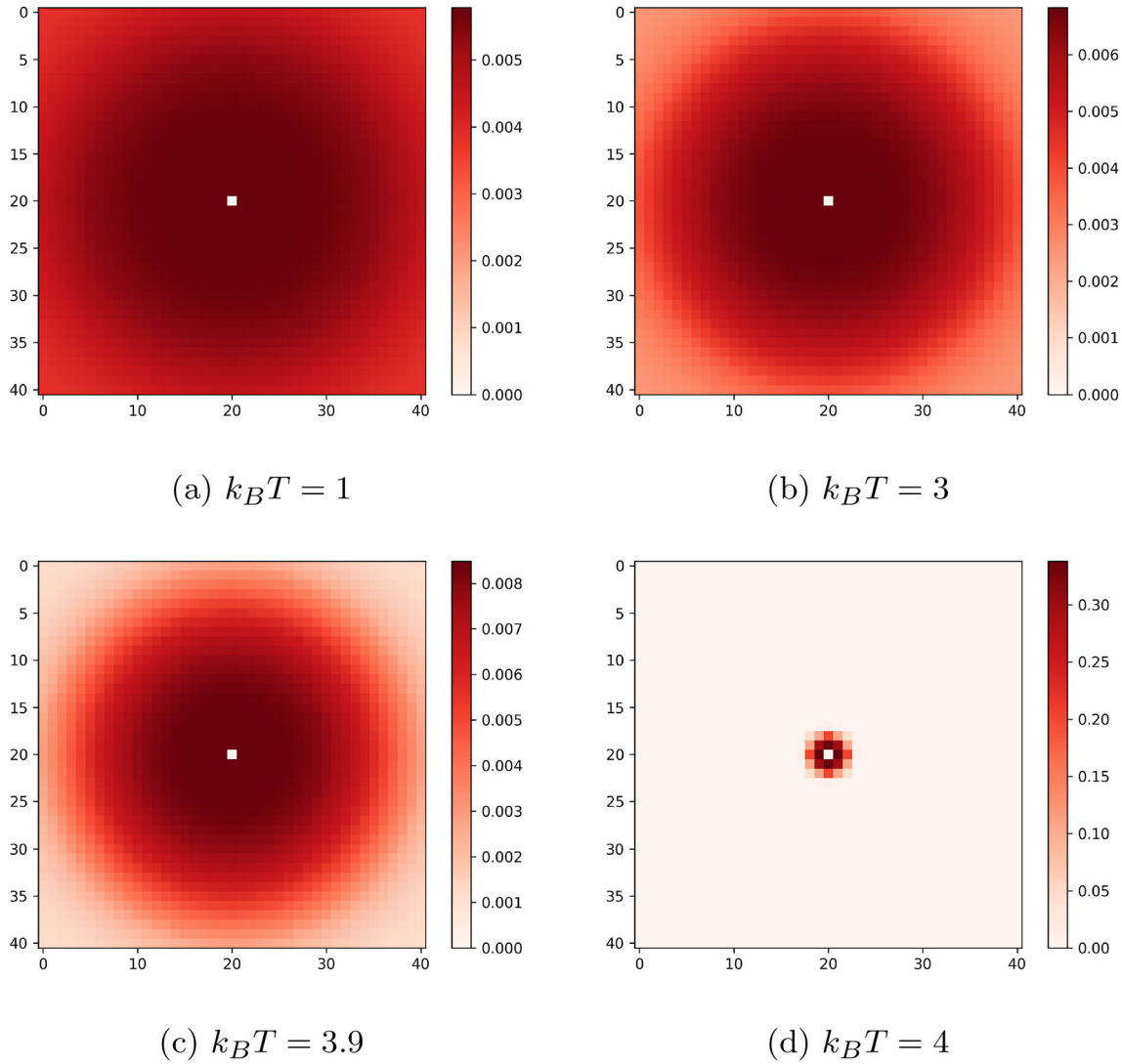

Fig. 2. Change of interaction strengths between the spins based on distance and temperature for a 20 × 20 lattice.

any case, the weight parameter, ω_j, representing the interaction strength, is defined based on this relation, while the temperature versus interaction strength is also defined using a Gaussian distribution. As a result, the following constraint is satisfied:

$$\omega_n \leq \omega_{n-1} \leq \omega_{n-2} \leq \cdots \leq \omega_3 \leq \omega_2 \leq \omega_1 \quad (2)$$

where n depends on the lattice size, ω_1 and ω_n represent the nearest and farthest neighbor interaction strengths, respectively. The long-range interactions between the magnetic spins are quantified through a window parameter (ω_n) varying based on the lattice size that covers every spin interaction on a lattice. The window parameter approach has been successfully applied previously to predict the spatio-temporal evolution of microstructures,[26,27] as well as to find the free energy of the Ising model.[28] In Fig. 2, the variation of the ω values can be observed for a 20×20 lattice. The matrix comprised of the ω values is ensured to have a size of $(2N+1) \times (2N+1)$ to be applicable for every spin even when its center is placed at the corner of the lattice. In addition, as described in Eq. 3, ω values are Gaussian distributed and normalized with respect to the total summation. The spin states are determined using this methodology. A visual schematic of the Ising model that accounts for both the nearest-neighbor and high-order interactions is shown in a 2D lattice in Fig. 3 for different values of $k_B T$.

$$\omega = \frac{\omega_1}{\sum_{i=1}^{n} \omega_i}, \frac{\omega_2}{\sum_{i=1}^{n} \omega_i}, \ldots, \frac{\omega_n}{\sum_{i=1}^{n} \omega_i} \quad (3)$$

Three-dimensional Ising Model

For any aforementioned state of the material, the problem of identifying the states of the spins is solved by defining the Hamiltonian expression with the utilization of the window approach. As in the 2D approach, if the dimension of the lattice is defined as $N \times N \times N$, up to the nth order interactions in the 3D neighborhood of the spin are considered. The use of this approach ensures that high-order interactions are accounted for to improve the accuracy and precision of the computations. To further improve the computational time efficiency and thus eliminate the associated scalability of the problem, the spin states in the 3D space are determined by solving the corresponding sub-problems in 2D plane sections. Accordingly, the 2D neighborhoods of the spin are obtained in x–y, x–z, and y–z plane sections, respectively. Next, the sub-problems are solved using the presented approach (for three different cases of temperature). If the plane-section solutions for the spin state are labeled as σ_i^{x-y}, σ_i^{x-z}, and σ_i^{y-z} for the x–y, x–z, and y–z plane sections, respectively, then the state of the spin, i, is determined by solving a secondary problem. In particular, the spin state in 3D is computed by deriving the following weighted-average expression:

$$\sigma_i = \text{sgn}\left(\frac{\left(\omega_i^{x-y} \times \sigma_i^{x-y}\right) + \left(\omega_i^{x-z} \times \sigma_i^{x-z}\right) + \left(\omega_i^{y-z} \times \sigma_i^{y-z}\right)}{\omega_i^{x-y} + \omega_i^{x-z} + \omega_i^{y-z}}\right) \quad (4)$$

where sgn is the sign function that is used to determine whether the state of the spin, σ_i, is spin-up (+ 1) or spin-down (− 1). The expression in Eq. 4 is developed explicitly in terms of the weightage parameters that are defined for each plane section (ω_i^{x-y} for x–y plane section, ω_i^{x-z} for x–z plane section, and ω_i^{y-z} for y–z plane section). For most cases, these weightage parameters are assumed to be equal, such that $\omega_i^{x-y} = \omega_i^{x-z} = \omega_i^{y-z} = 1$ (assuming that the neighboring spins in different plane sections contribute to the spin state equivalently). Maintaining the explicit definition of the weightage parameters is beneficial for cases when the neighboring spin information in a certain plane section becomes more decisive in than the other planes.

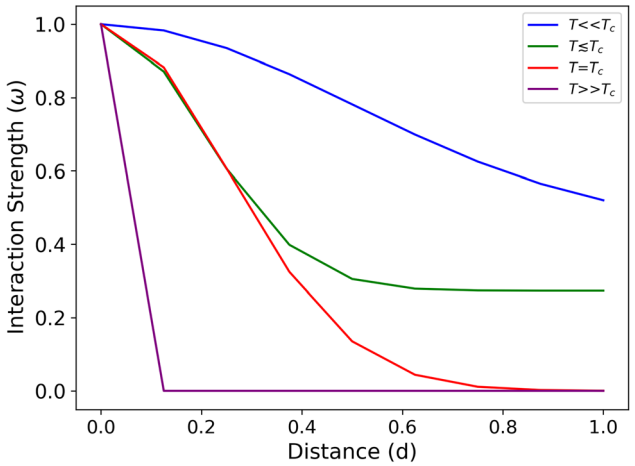

Fig. 3. Change of interaction strengths between the spins based on distance and temperature for a 4×4 lattice.

RESULTS AND DISCUSSIONS

Model Verification with Theoretical Results

The Ising model was initially devised using a 4×4 lattice as a foundational case. In an effort to validate the constructed model, the magnetization parameter, designated as M, is computed, and its relationship with the free energy is depicted graphically in Fig. 4, considering the interactions of spins within the influence of an external magnetic field. It becomes crucial to encompass all potential configurations of the spins. For this 4×4 domain, 65,536 distinctive magnetic spin arrangements exist. The numerical magnetization parameter is computed for all these combinations employing Eq. 4. Subsequently, theoretical solutions for the magnetization parameter are calculated across a spectrum of external magnetic field values, utilizing Eq. 5. Proceeding further, the free energy (F) of the system is ascertained using Eq. 6.[16] This equation computes both theoretical and computational M values. The equation has its foundations in the mean field theory, which only considers the nearest neighbors

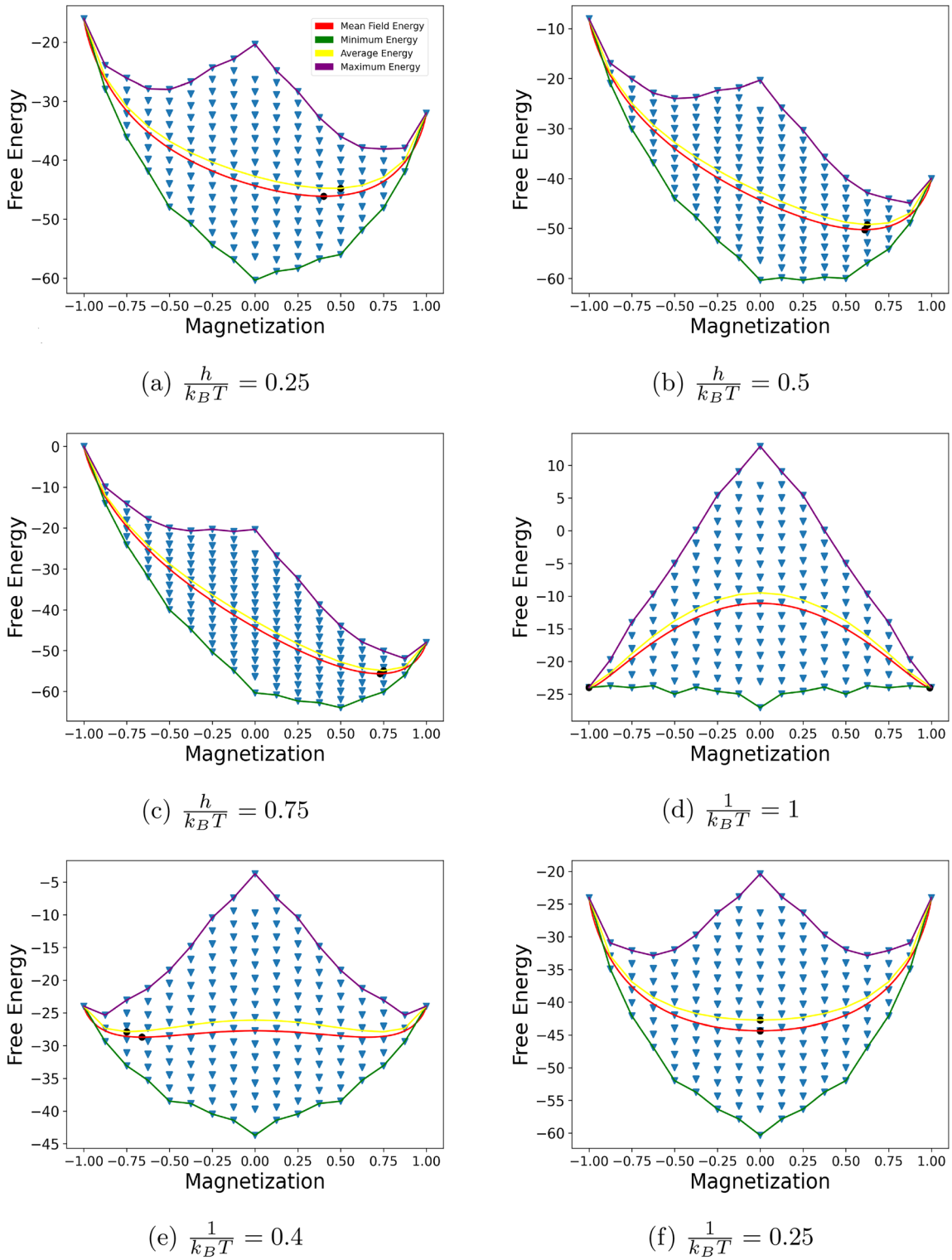

Fig. 4. The change in the free energy (*F*) as a function of the magnetization parameter (*M*) for interacting spins and with an external magnetic field as the temperature is constant (a–c) and varying temperature as the external magnetic field is constant (d–f). The blue samples show the exhaustive solution data (Color figure online).

on a lattice, irrespective of temperature variations. This method proves invaluable when dealing with large domain sizes, given the impracticality of calculating the free energy for each possible spin configuration. While the mean field theory is proficient in generalizing behavior, it does lack precision due to the absence of long-range neighbor data. In an attempt to draw a fair comparison between the theory and the long-range neighbor approach, the same methodology is employed, albeit

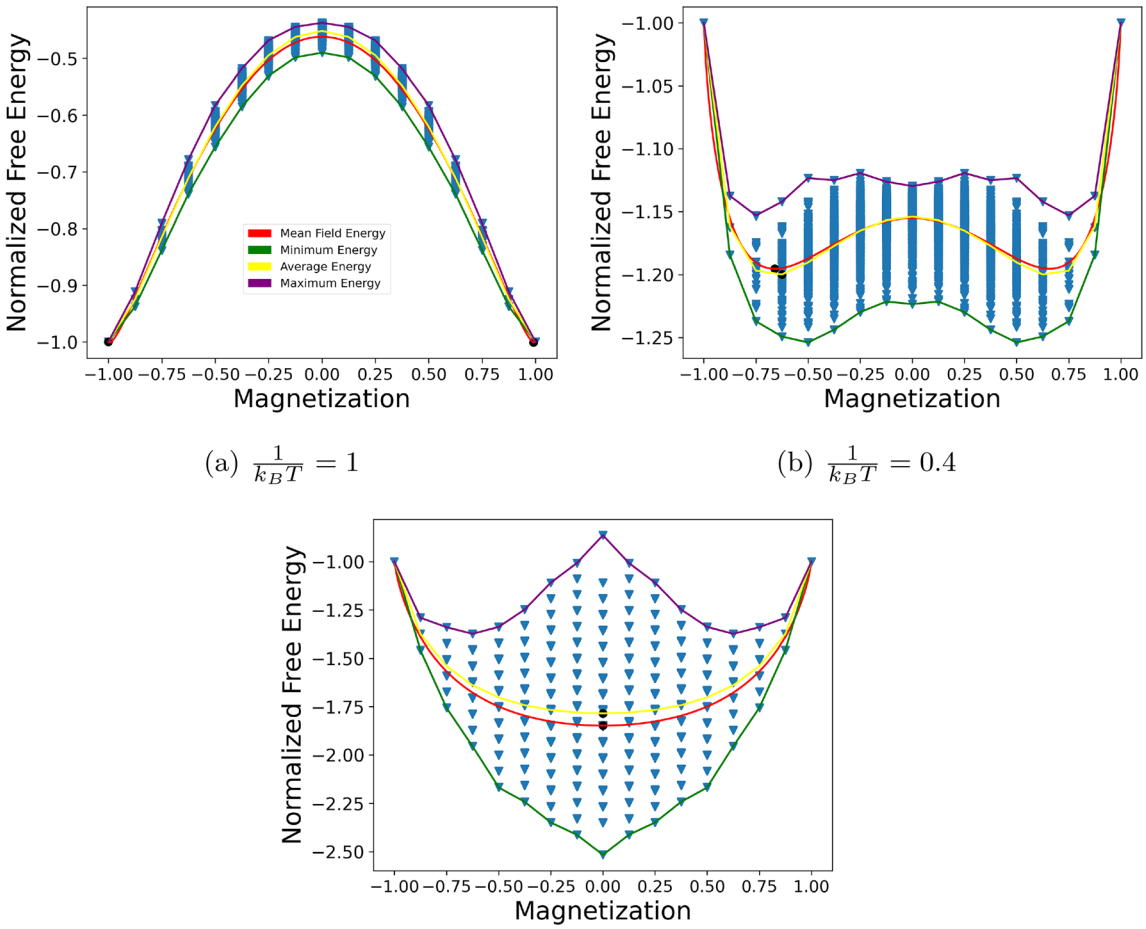

(a) $\frac{1}{k_B T} = 1$ (b) $\frac{1}{k_B T} = 0.4$

(c) $\frac{1}{k_B T} = 0.25$

Fig. 5. The change in the free energy (F) as a function of the magnetization parameter (M) for long-range interacting spins and with varying temperature as the external magnetic field is constant. The blue samples show the exhaustive solution data (Color figure online).

with certain adjustments. Importantly, the interaction strength matrix is designed to only consider the nearest neighbors, mirroring the fundamental assumption of the mean field theory. Due to the potential for multiple spin combinations to exhibit the same count of positive and negative spins, the overlap results in only a fraction of the total 65,536 combinations being visible in the plotted diagrams. Additionally, it is demonstrated that the minimum free energy observed in both numerical and theoretical solutions tends to occur at nearly identical magnetization levels. This observation adds further validation to the methodology employed in the study.

$$M = \frac{N_P - N_N}{N} \tag{5}$$

where N_P is the number of positive spins (upward), N_N is the number of negative spins (downward), N is the total number of spins in a lattice, and M stands for the magnetization.

$$M = tanh\left(\frac{h}{k_B T}\right) \tag{6}$$

where k_B is the Boltzmann constant and T is the temperature. The value of M must remain within -1 to 1. The free energy expression is given as follows:[7]

$$\frac{F(M)}{Nk_B T} = -\left(\frac{J_q q}{2k_B T}\right)M^2 - \left(\frac{h}{k_B T}\right)M + \left(\frac{1+M}{2}\right)log\left(\frac{1+M}{2}\right) + \left(\frac{1-M}{2}\right)log\left(\frac{1-M}{2}\right) \tag{7}$$

where J_q is the constant interaction strength and q is the coordination number of the lattice, which is 4 for a 2D lattice. The first two terms in the equation represent the interaction energy. The following terms constitute the entropy equation. The corresponding magnetization to the minimum of the free energy curve is the magnetization level the system will have.

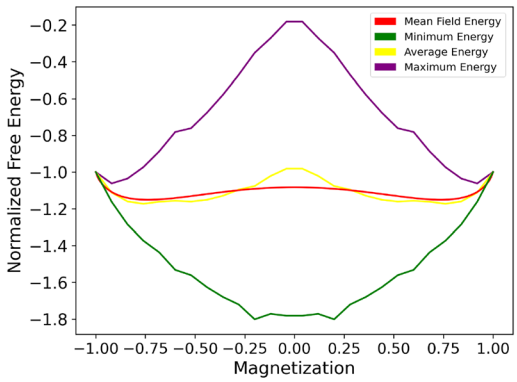

(a) Simple average with the nearest-neighbor approach

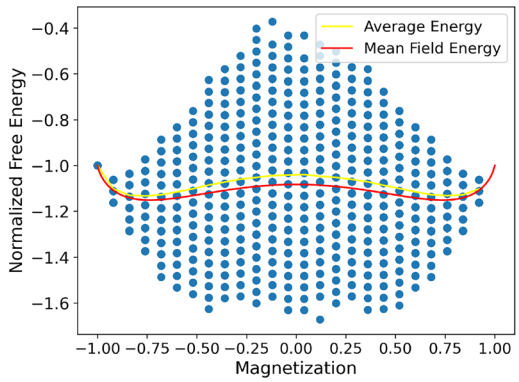

(b) Average of random combinations (blue samples) with the nearest-neighbor approach

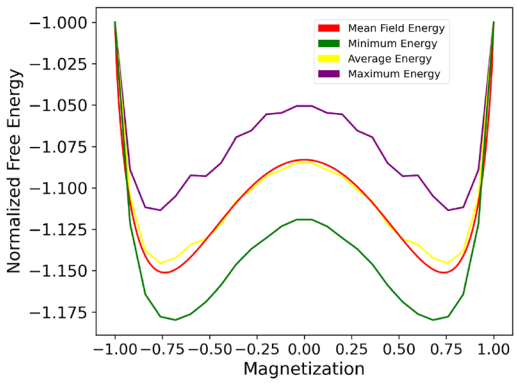

(c) Simple average with the long-range neighbor approach

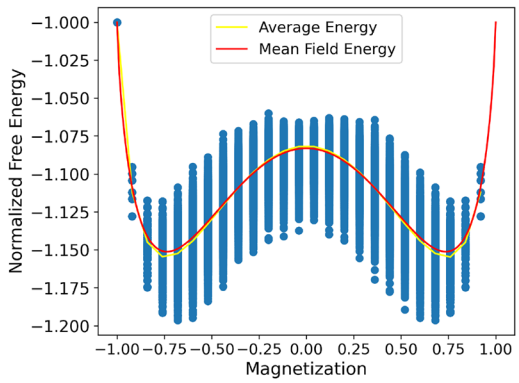

(d) Average of random combinations (blue samples) with the long-range neighbor approach

Fig. 6. Comparison of the average of the numerical results against the theoretical solution with two different approaches for a 5×5 lattice: Simple average and the average of the random combinations where $k_B T = 2.5$ (Color figure online).

Extended Mean Field Solution to the Ising Model

The mean field theory is a well-established technique in physics that offers credible approximations to precise solutions when the dimensional count is sufficiently high. It is the preferred estimation strategy for modeling systems characterized by interactions.[16] However, it is important to acknowledge that the solutions derived from the mean field theory do rest on certain suppositions concerning the correlations amidst interacting spins. In utilizing this approach, the spin state is discerned on the basis of the system's free energy, which is a function of the Hamiltonian. In the course of determining the explicit representation of the system's free energy, the covariance relationship among the spins over long range is typically disregarded, primarily because of the computational challenges and expenses associated.[16,29,30]

This study seeks to enhance the mean field solution by dispensing with this fundamental presumption, a step that is imperative to the quantification of uncertainties within the external magnetic fields. With the application of the weight parameter approach, the free energy levels deviate from those associated with the nearest neighbor, a phenomenon illustrated in Fig. 5. The divergence is considerably less pronounced at lower temperatures, yet it escalates when the temperatures are higher.

Extension of the Ising Solution to Large Computational Domains

It is important to investigate the behavior of larger domains as well since it is unlikely to represent the sufficient number of spins with a simple lattice that is of size 4×4. However, unlike mean field theory, whose computational time is not

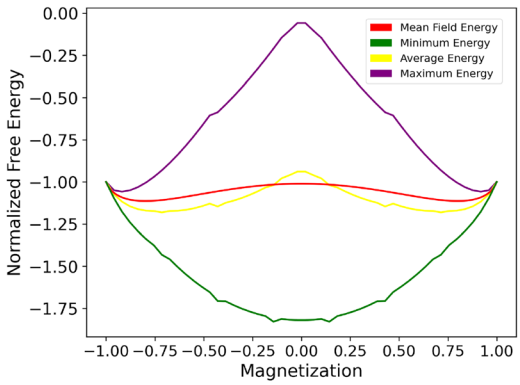

(a) Simple average with the nearest-neighbor approach

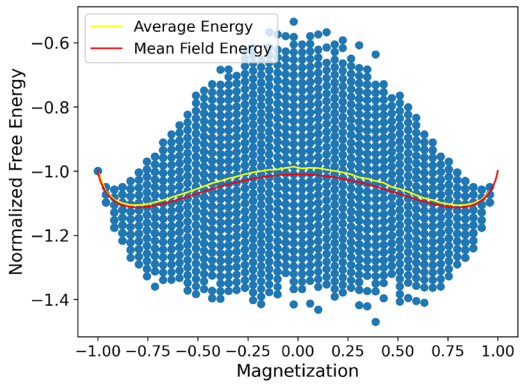

(b) Average of random combinations (blue samples) with the nearest-neighbor approach

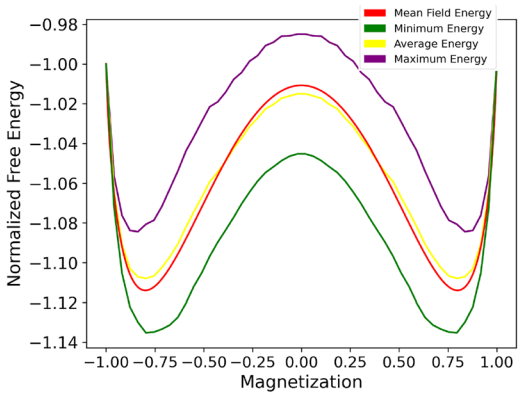

(c) Simple average with the long-range neighbor approach

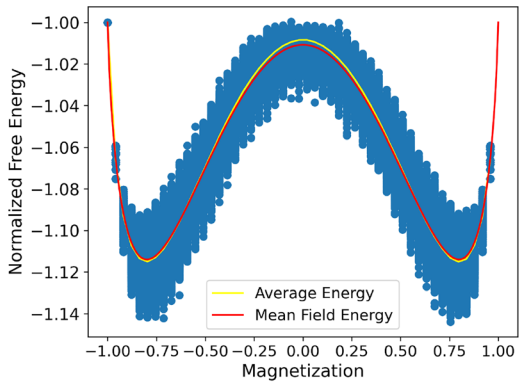

(d) Average of random combinations (blue samples) with the long-range neighbor approach

Fig. 7. Comparison of the average of the numerical results against the theoretical solution with two different approaches for a 7×7 lattice: Simple average and the average of the random combinations where $k_B T = 2.5$ (Color figure online)

affected by the size of the lattice, the long-range neighbor method requires a different approach. As any size of lattice $> 4 \times 4$ would lead to an excessive number of combinations resulting in extreme computational cost; two methods are applied to evaluate the magnetization under a certain temperature and external magnetic field, thus the phase transition. The first one is the simple average where the average is obtained only using the minimum and maximum free energy levels. The second approach is to perform the calculations on randomly selected combinations. This is applied for lattices with the size of 5×5 in Fig. 6, 7×7 in Fig. 7, and 9×9 in Fig. 8 for a temperature that is close to the phase transition zone ($k_B T = 2.5$).

To indicate the differences and applicability of the methods, the results are obtained for both nearest-neighbor and long-range neighbor approaches. The simulations conducted in this study have produced notable findings that contribute to our understanding of the phase transition behavior in ferromagnetic materials. Importantly, it was discovered that the random selection of certain spin combinations can yield an average magnetization that exhibits a strong correlation with the mean field theory predictions. This correlation was observed in both considered cases, demonstrating the validity of the mean field theory in the modeling of such systems. Moreover, it was found that the influence of long-range neighbors is a significant factor. When these interactions are relatively higher, the simple average calculation aligns remarkably well with the mean field theory predictions. This observation underscores the importance of considering long-range interactions in modeling the magnetic properties of these materials. However, a different scenario unfolds when only the nearest neighbors are considered. The results gleaned from the simple average calculation in this situation tend to be misleading. As per our expectations, the variation observed in this case was found to be lower. This outcome emphasizes the

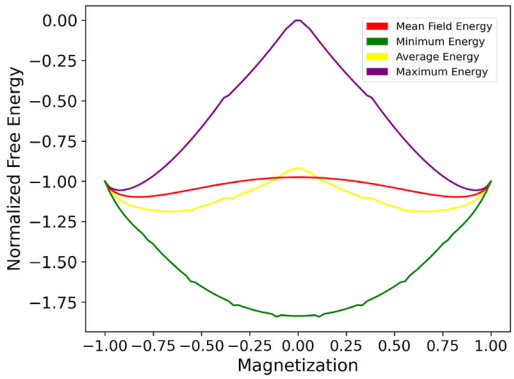

(a) Simple average with the nearest-neighbor approach

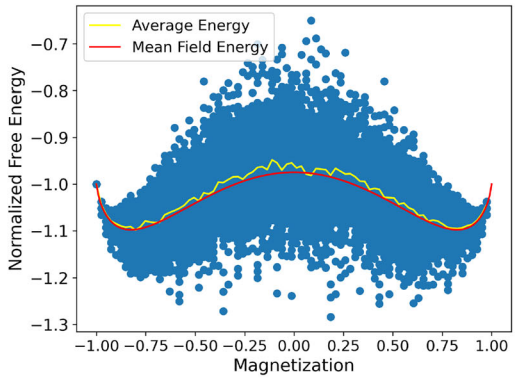

(b) Average of random combinations (blue samples) with the nearest-neighbor approach

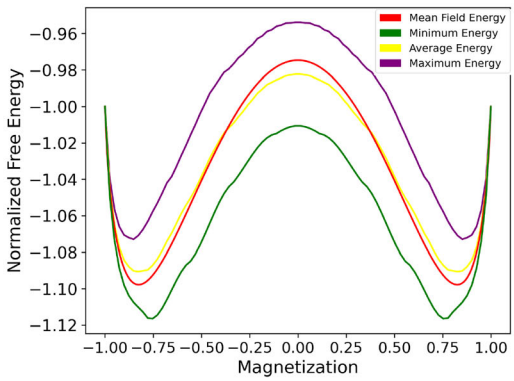

(c) Simple average with the long-range neighbor approach

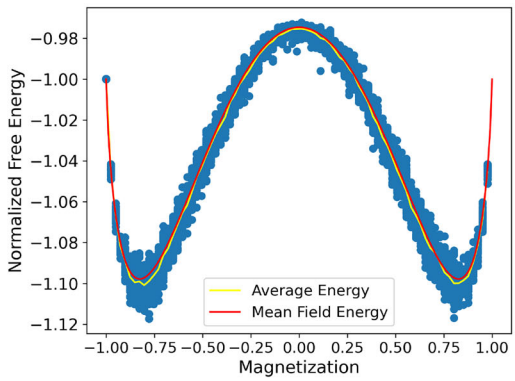

(d) Average of random combinations (blue samples) with the long-range neighbor approach

Fig. 8. Comparison of the average of the numerical results against the theoretical solution with two different approaches for a 9×9 lattice: Simple average and the average of the random combinations where $k_B T = 2.5$ (Color figure online)

crucial role of more distant spin interactions in understanding the system's behavior.

Another important finding pertains to the impact of lattice size on the system's magnetization. As the lattice size increases, a visible change in the system's magnetization becomes apparent. The larger the lattice size, the higher the magnetization of the system will be. This relationship elucidates the importance of system size in determining its magnetic behavior. Interestingly, as the lattice size grows, the resulting magnetization curves become smoother. This result demonstrates the system's ability to stabilize and produce more predictable outcomes as its size expands, further reinforcing the significance of the lattice size in the study of such systems. One striking revelation from this study was the computational efficiency of finding only the maximum and minimum free energy levels compared to using a random example approach. We found that the disordered spin combinations, i.e., the ones with spins in the most chaotic arrangements, are likely to possess the maximum free energy. Conversely, the most ordered spin combinations—those in which the spins are neatly arranged—tend to have the minimum free energy. These findings provide a valuable perspective on the computational advantages and physical insights to be gained from focusing on the extreme ends of the free energy spectrum. By understanding the nuances of this relationship, we can build more effective and efficient models for the exploration of phase transitions in ferromagnetic materials.

Three-Dimensional Ising Model Development

The 3D Ising model extends the principles used in 2D domains, particularly employing the window approach to model the intricate higher order interactions between the magnetic spins. This window approach method, a widely used technique for modeling spin states in 2D domains, is thus co-opted for the creation of 3D Ising model

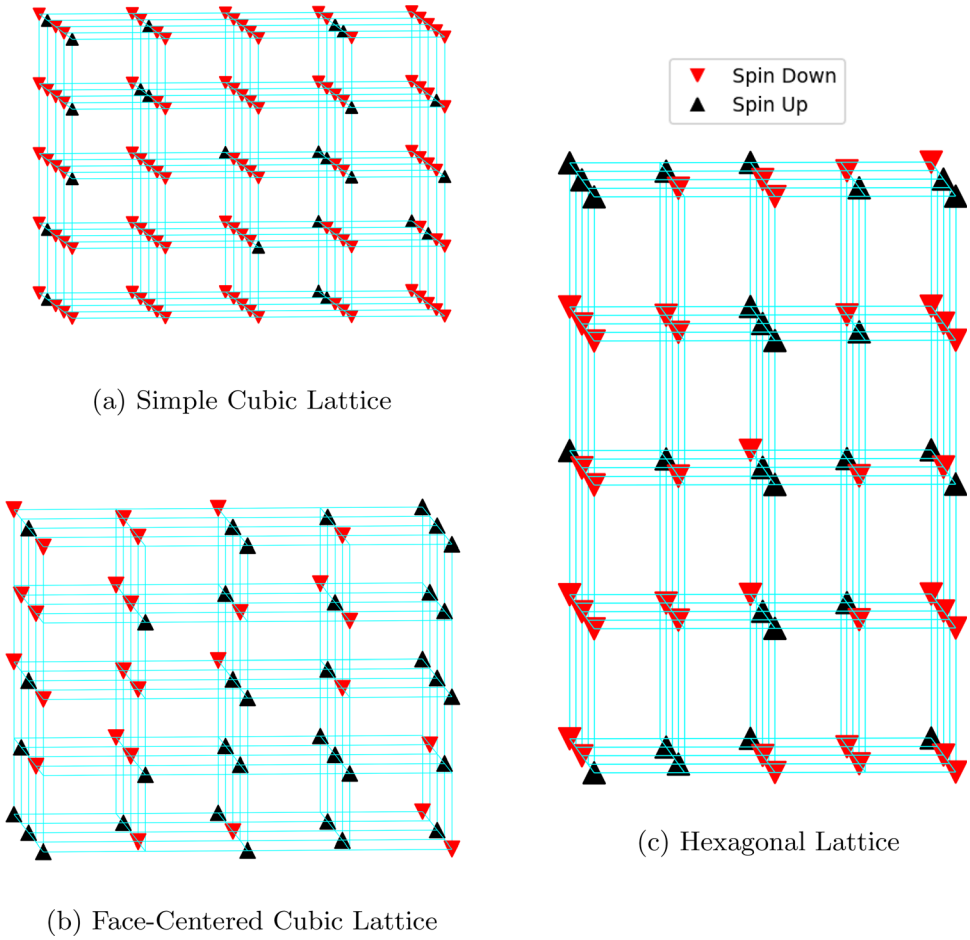

Fig. 9. Example scaled visualization of the 3D lattice structures.

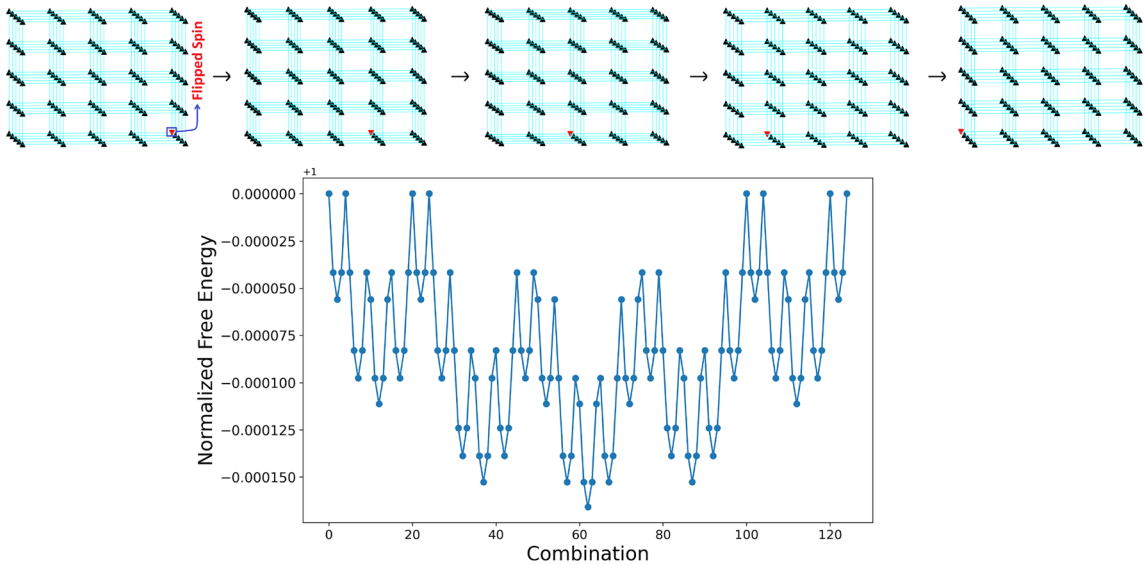

Fig. 10. Variation of the free energy of the combinations where there is only one flipped spin for a $5 \times 5 \times 5$ simple cubic lattice

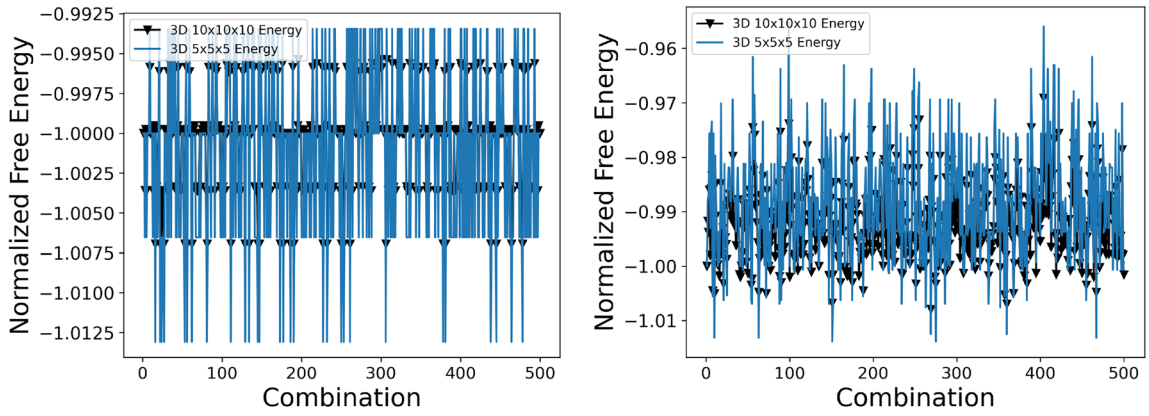

(a) $Magnetization = \frac{124}{125}$ (b) $Magnetization = \frac{123}{125}$

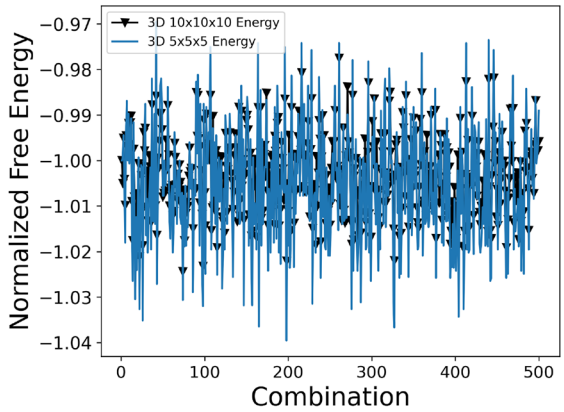

(c) $Magnetization = \frac{122}{125}$

Fig. 11. Free energy of the combinations for simple cubic lattices with the size of $5 \times 5 \times 5$ and $10 \times 10 \times 10$ for different magnetization levels.

representations. The focus is primarily on understanding the spin state of the material and how the various interactions might influence the overall magnetic properties. In the context of 3D structures, three distinct lattice types are considered: the simple cubic, the face-centered cubic, and the hexagonal lattices. These lattice structures, scaled for clarity, are depicted in Fig. 9. Each one offers unique insights into the arrangement and interactions of spins within a ferromagnetic material.

The simple cubic lattice, as the name suggests, presents a straightforward structure with spins at every site within the lattice. It offers a robust foundation upon which to understand the basic principles of spin-spin interactions within a 3D space. It is a fundamental structure in the realm of the 3D Ising model. On the other hand, the face-centered cubic lattice is derived from the simple cubic structure with some modifications. In this lattice, certain spins are omitted from the simple cubic structure. This strategic omission is carried out to maintain the applicability of the window approach across all layers in the structure. Although these sites are vacant, they still bear a corresponding interaction strength value within the window. However, since there are no spins at these sites, the interaction strength is effectively nullified as it is multiplied by zero. This specific design ensures that there are no adjacent spins along any line in the structure in every dimension of the face-centered cubic lattice. The third lattice structure explored is the hexagonal lattice. From a top-view perspective, the upper layer of the hexagonal lattice appears strikingly similar to the face-centered cubic lattice. However, as one moves downwards through the layers, the hexagonal structure remains constant, unlike the face-centered cubic structure. Additionally, the distances between the sites vary, marking another departure from the face-centered cubic and simple cubic structures. The inner portion of the lattice, the core of the hexagonal structure, repeats as the size increases. Consequently, the hexagonal lattice possesses a unique structure compared to the regular hexagonal lattice. For a fair comparison, all the lattice structures are selected with the same outer dimension,

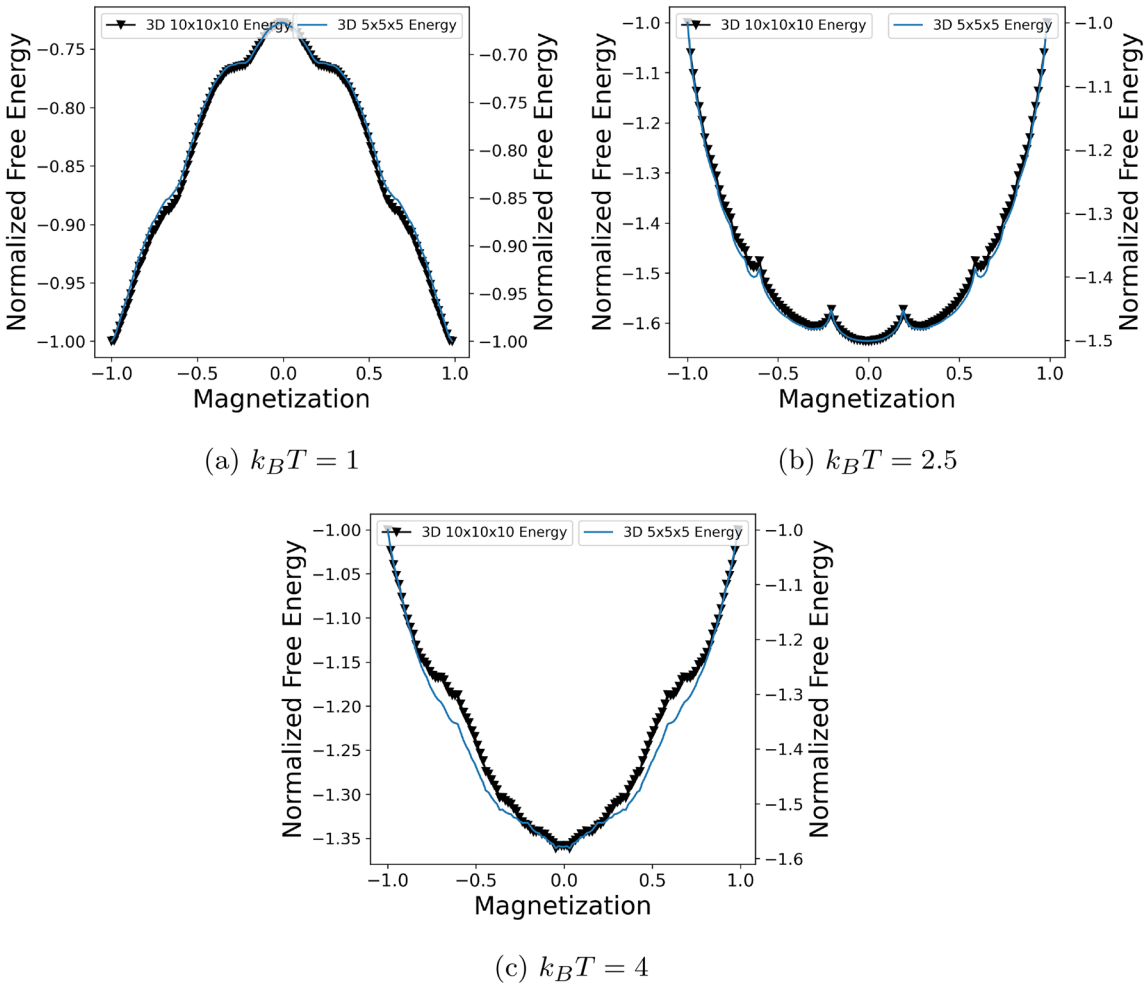

(a) $k_BT = 1$ (b) $k_BT = 2.5$

(c) $k_BT = 4$

Fig. 12. Free energy versus magnetization for simple cubic lattices with the sizes of $5 \times 5 \times 5$ and $10 \times 10 \times 10$ for different temperatures.

specifically a value of 5. By maintaining this uniformity in outer dimensions, it becomes possible to accurately compare and contrast the spin-spin interactions and overall magnetic behavior within the different lattice structures.

First, the window approach is applied to the simple cubic lattice particularly to investigate the effect of the boundary condition. A case study is created where all possible combinations of magnetization = $\frac{124}{125}$ are considered and their free energies are calculated. The purpose is to observe the change in the free energy based on the flipped spin location in the lattice to explore the domain size dependence of the problem physics. The lattices in Fig. 10 are the first few combinations that the calculation performed. When the flipped spin is in the corner sites of the lattice, the free energy is the highest as expected as it interacts with fewer spins. Since the disruption causes a fall in free energy, when the flipped spin interacts with the most spins with high interaction strength, it is observed that the free energy is the lowest. This is the case where it is located in the center of the lattice. Even though the free energy variation occurs, it is quite low for this case, indicating that even for a lattice of small size ($5 \times 5 \times 5$), the solution does not vastly depend on the domain size.

Next, another case is created to further investigate this effect. However, in this case, there are more flipped spins in the system as shown in Fig. 11. Free energies of lattices with the size of $5 \times 5 \times 5$ and $10 \times 10 \times 10$ are compared to decide on the minimum lattice size that can generate satisfactory results since larger lattices in 3D cause even more computational burden. There are more possible spin combinations for the system when more flipped spins are present, and 500 of these combinations are selected randomly for the lattice with a size of $10 \times 10 \times 10$ in (a) and both lattices in (b) and (c). For comparison, some of the combinations of the lattice with a size of $5 \times 5 \times 5$ are repeated in (a). The smaller lattice is considered to represent the bounds as their free energies are prone to have values within a greater range. The larger lattices have free energy values that are more confined for the same magnetization level since the number of

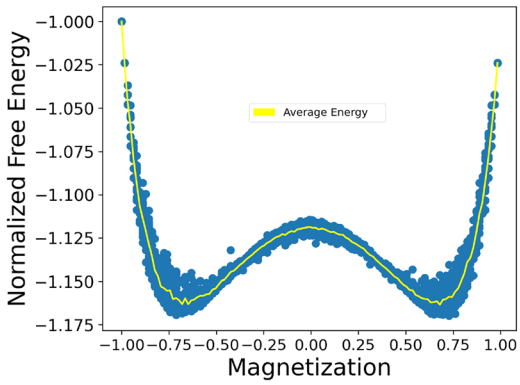

(a) Simple Cubic Lattice where $k_BT = 1$

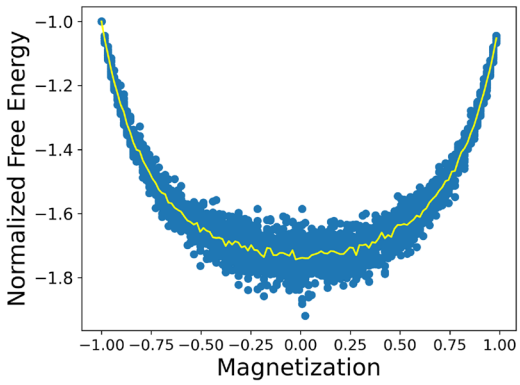

(b) Simple Cubic Lattice where $k_BT = 4$

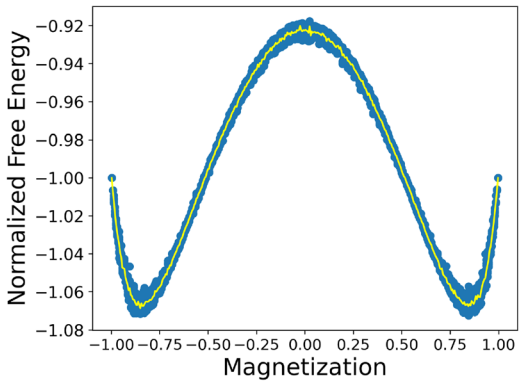

(c) Face-Centered Cubic Lattice where $k_BT = 1$

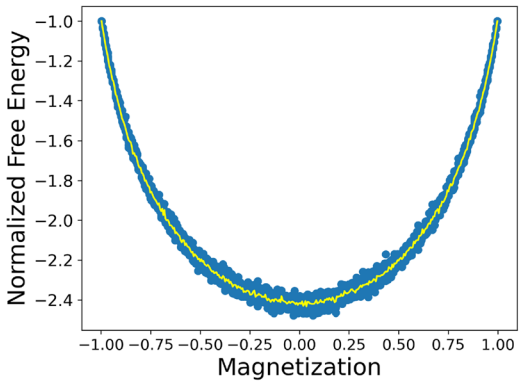

(d) Face-Centered Cubic Lattice where $k_BT = 4$

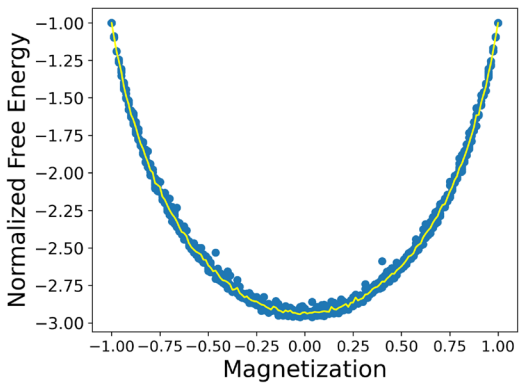

(e) Hexagonal Lattice where $k_BT = 1$

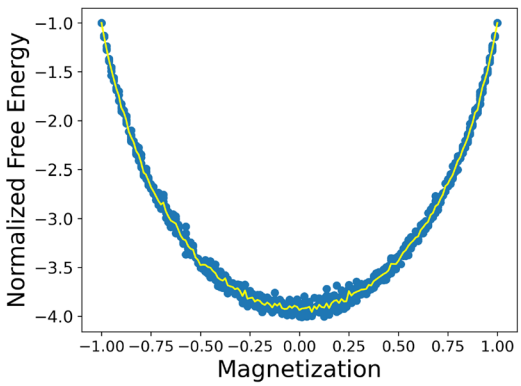

(f) Hexagonal Lattice where $k_BT = 4$

Fig. 13. Free energy versus magnetization curves under different temperatures for different 3D structures.

affected spins increases with size. That causes the effect of the flipped spins to diminish, resulting in less variation in the free energy. The variation also increases when the number of flipped spins is higher because of the combination variety. Even though the variation decreases with size, the small difference between the lattices for all cases shows that using the lattice with a size of $5 \times 5 \times 5$ will be able to accomplish a base for the simulation.

The comparison is then made between the lattices with different sizes for the same type of combinations. The $10 \times 10 \times 10$ lattice is created by

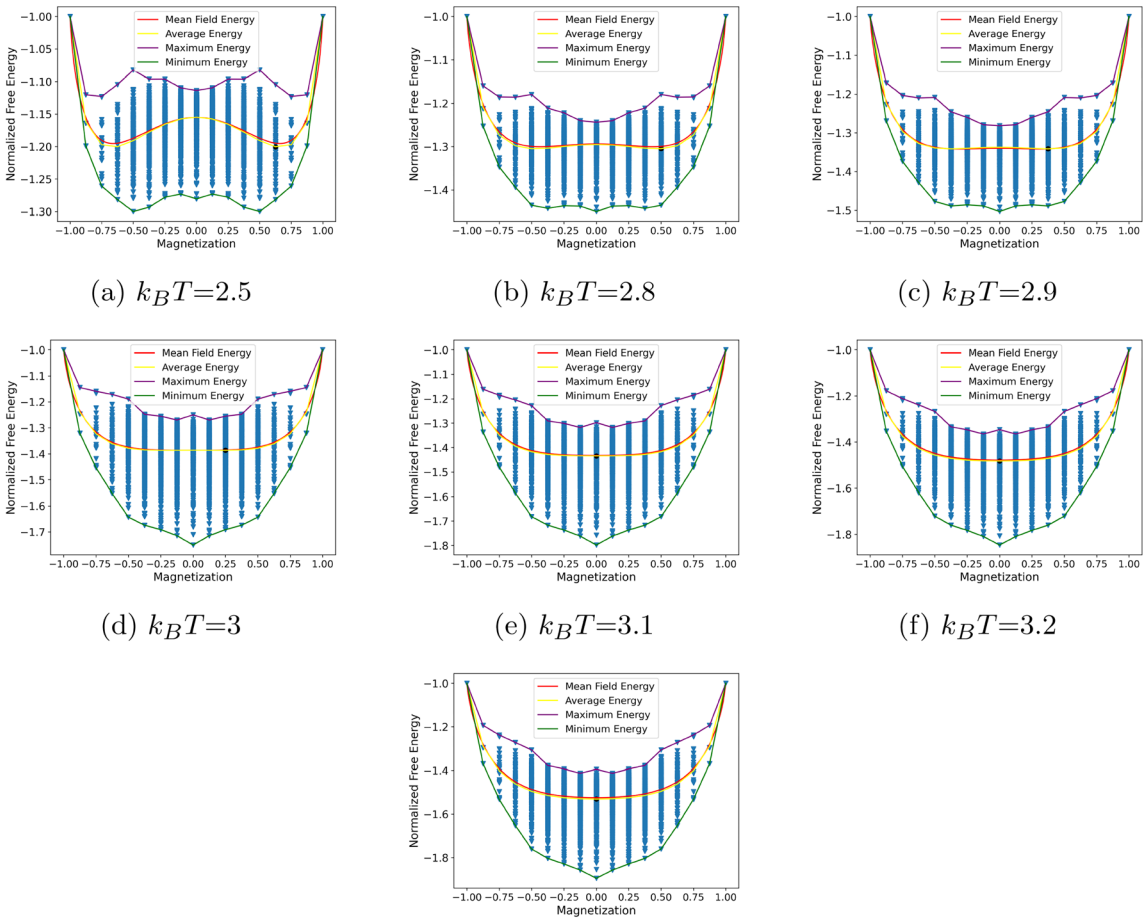

(a) k_BT=2.5 (b) k_BT=2.8 (c) k_BT=2.9

(d) k_BT=3 (e) k_BT=3.1 (f) k_BT=3.2

(g) k_BT=3.3

Fig. 14. Change of free energy versus magnetization for a 4 × 4 lattice under different k_BT values, particularly close to the phase transition region. These distributions are going to be used for uncertainty analyses.

combining eight identical lattices with size $5 \times 5 \times 5$. For each magnetization level, only one combination is selected and investigated for different temperatures. The selection of the combination type is loosely based on the findings of the minimum free energy in 2D. The results in Fig. 12 show that regardless of the lattice size, a similar behavior can be observed between the free energy and magnetization even though the values vary.

Finally, the simple cubic, face-centered, and hexagonal lattices with the size of $5 \times 5 \times 5$ are studied to generate outcomes with varying magnetization values. Since the combination number increases even faster in 3D, the purpose is to select the smallest lattice size as the representative volume element (RVE) size for preliminary evaluation. Here, the goal is to use the RVE as a periodically repeating structure when modeling very large computational domains. The size is preserved for the other lattice structures as shown in Fig. 9. The free energy values for these structures are investigated under different temperatures as shown in Fig. 13. For all of them, the idea of the average of random combinations is used, even though it cannot be validated as it was in the 2D case since the mean field theory is valid for only 2D. For simple and face-centered cubic structures, the phase transition occurs between the given k_BT values in Fig. 13. For the hexagonal lattice, the transition seems to occur at a lower temperature than the presented values in Fig. 13.

Uncertainty Analysis

The effects of the uncertainties arising from the external magnetic field and temperature are investigated for a 4×4 2D lattice. The investigation space for temperature is chosen to be between k_BT = 2.5 and k_BT = 3.3. The phase transition occurs at k_BT = 3 yet the transition starts around k_BT = 2.5. The free energy of the combinations under certain temperatures is given in Fig. 14. Even though the minimum of average free energies provides an intuition about the magnetization that the system will have, it can be observed that it is

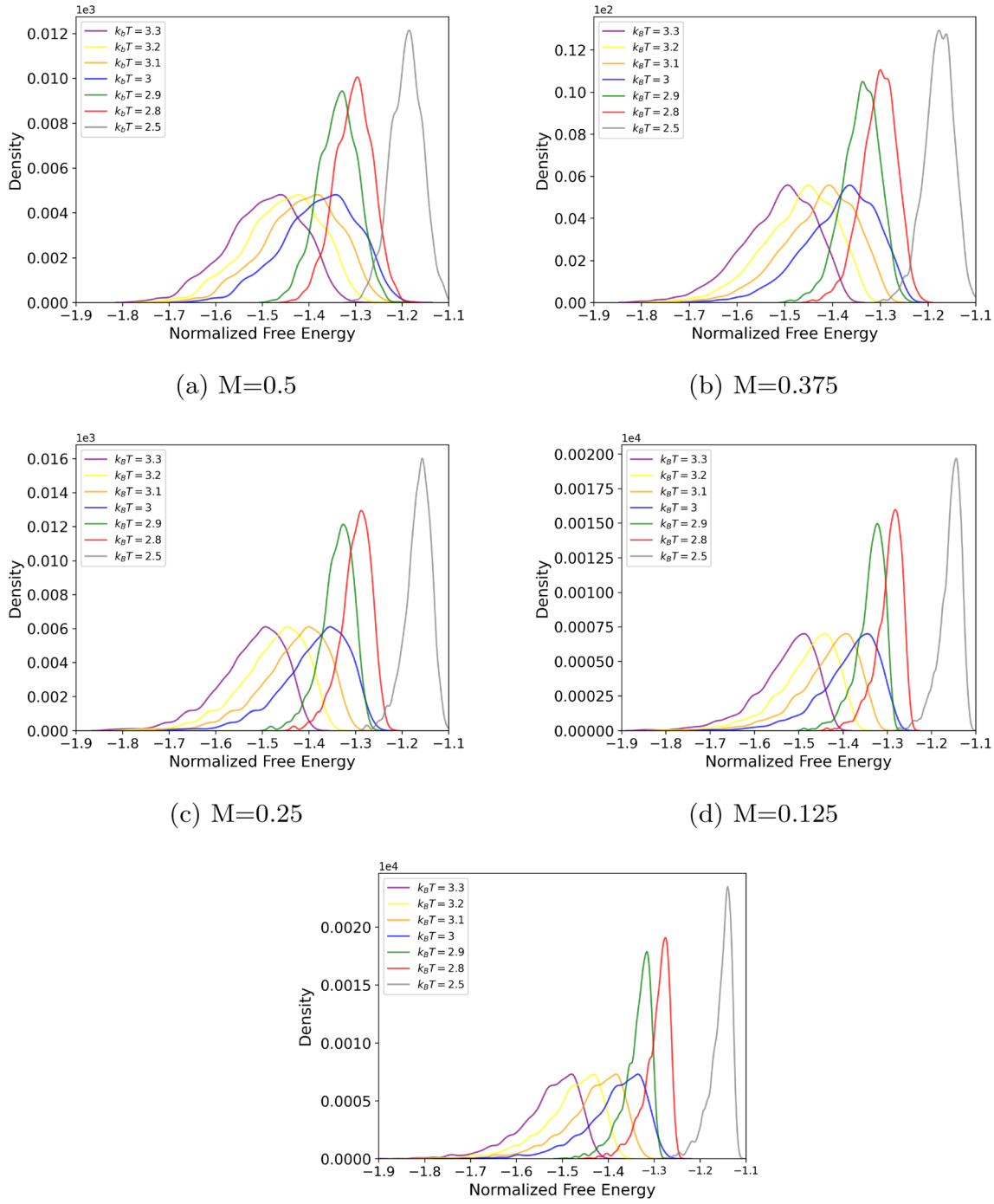

Fig. 15. The effects of uncertainty arising from the temperature on the free energy values associated with the phase transition behavior for different magnetization levels. Transition behavior starts at $k_BT = 2.5$ and occurs around $k_BT = 3$.

actually a probability distribution. For that reason, the minimum of the free energies shows the magnetization of the most probable final combination. To further investigate these probability distributions, the histogram of the combinations is generated regarding the free energies as shown in Fig. 15. The distributions are obtained for different k_BT values and for five different magnetization levels to observe the shift of the distributions. When the k_BT is lower than the transition temperature, the expected value for the magnitude of the normalized free energy decreases, which is parallel to the findings obtained before. Similarly, the expected value for the magnitude of the normalized free

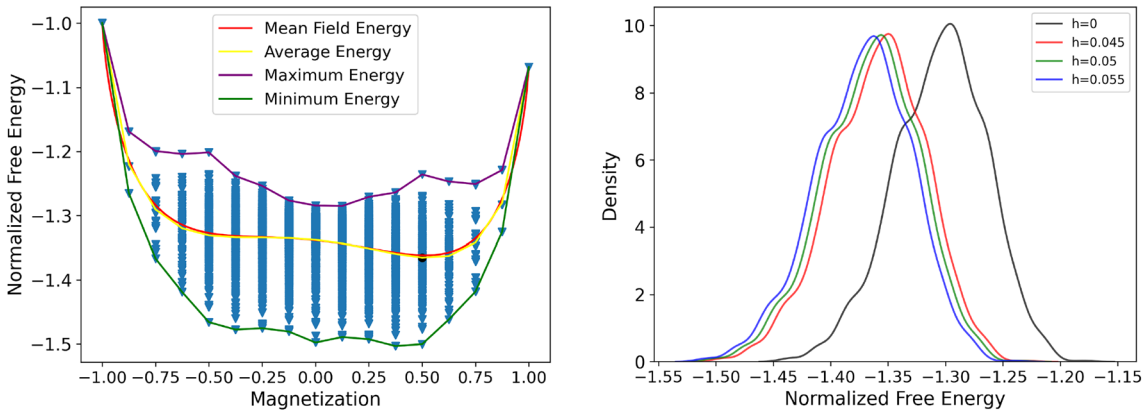

(a) (b)

Fig. 16. Uncertainty effect of external magnetic field for the system that is close to phase transition temperature. Since the uncertainty is not strong to alter the magnetization of the system, only the density curve for $M = 0.5$ is shown.

energy increases as $k_B T$ increases. Moreover, the type of distribution does not change for the cases where $k_B T$ is greater than the transition temperature, yet the standard deviation becomes lower. As the $k_B T$ values increase, the standard deviation values for the normalized free energy increase as well. This finding indicates that the effects of uncertainty related to temperature become more prevalent at higher temperatures. In other words, the phase transition behavior is more predictable at lower temperature values with the decrease in the standard deviation of the free energy values.

Secondly, the uncertainty arising from the external magnetic field is considered as illustrated in Fig. 16. For this study, the temperature value is kept constant at a value that is close to the transition value. The type of probability distribution for a magnetization level that is equal to 0.5 stays the same for each case. It is also observed that the standard deviation values for these distributions do not demonstrate any meaningful changes. Increasing the external magnetic field causes the free energy levels to be lower. In summary, the uncertainty arising from the external magnetic field propagates on the free energy similarly even for different magnetization levels while the expected values can be different as a result of the changes in magnetization.

CONCLUSION

In this research, we have effectively modeled the phase transition of ferromagnetic materials using 2D and 3D Ising models. These models successfully incorporated the intricate long-range magnetic spin-spin interactions and the presence of an external magnetic field. We have also integrated an UQ formulation into the Ising models, which helped us assess the uncertainties associated with the external magnetic field and temperature. Importantly, we were able to evaluate the implications of these uncertainties on the phase transition from a ferromagnetic to a paramagnetic state. Our work acknowledges the existing complexities in the Ising model, particularly in its three-dimensional version, which still lacks a universally accepted solution. We have reiterated the limitations of current experimental methods and emphasized the need for models like ours that can interpret experimental results. Overall, this study contributes to the ongoing research in the field of phase transitions of ferromagnetic materials. We believe our findings will support future research that seeks to refine and enhance the understanding of phase transitions, particularly in the context of complex three-dimensional systems.

ACKNOWLEDGEMENTS

The authors acknowledge the financial support from the Air Force Office of Scientific Research (AFOSR) Young Investigator Program under Grant FA9550-21-1-0120.

CONFLICT OF INTEREST

On behalf of all authors, the corresponding author states that there is no conflict of interest.

OPEN ACCESS

REFERENCES

1. D. Jiles, Recent advances and future directions in magnetic materials. *Acta Materialia* 51(19), 5907 https://doi.org/10.1016/j.actamat.2003.08.011 (2003).
2. O. Gutfleisch, M.A. Willard, E. Brück, C.H. Chen, S. Sankar, and J.P. Liu, Magnetic materials and devices for the 21st century: stronger, lighter, and more energy efficient. *Adv. Mater.* 23(7), 821 https://doi.org/10.1002/adma.201002180 (2011).
3. W. Zia and M.S. Anwar, *Magnetic Phase Transitions (Electricity and Magnetism)* (2013).
4. G. Qiao, G. Liu, Z. Shi, Y. Wang, S. Ma, and T.C. Lim, A review of electromechanical actuators for more/all electric aircraft systems. *Proc. Inst. Mech. Eng. Part C J. Mech. Eng. Sci.* 232(22), 4128 (2018).
5. M.S.S. Kazmin, *Ising Model in Three Dimensions with Long-Range Power-Law Correlated Site Disorder: A Monte Carlo Study* (2022).
6. R.A. Serway and J.W. Jewitt, *Physics for Scientists and Engineers with Modern Physics Volume I—Technology Update*, 10th Edn., pp. 742–771 (2019).
7. J.V. Selinger and J.V. Selinger, Ising model for ferromagnetism, in *Introduction to the Theory of Soft Matter: From Ideal Gases to Liquid Crystals*, pp. 7–24 (2016).
8. E. Ising, Beitrag zur theorie des ferromagnetismus. *Zeitschrift für Physik* 31(1), 253 (1925).
9. L. Onsager, Crystal statistics. I. A two-dimensional model with an order-disorder transition. *Phys. Rev.* 65(3–4), 117 (1944).
10. J.W. Britton, B.C. Sawyer, A.C. Keith, C.-C.J. Wang, J.K. Freericks, H. Uys, M.J. Biercuk, and J.J. Bollinger, Engineered two-dimensional Ising interactions in a trapped-ion quantum simulator with hundreds of spins. *Nature* 484(7395), 489 https://doi.org/10.1038/nature10981 (2012).
11. S. Bornholdt, Expectation bubbles in a spin model of markets: intermittency from frustration across scales. *Int. J. Mod. Phys. C* 12(05), 667 https://doi.org/10.1142/S0129183101001845 (2001).
12. A.W. Sandvik, Computational studies of quantum spin systems, in *AIP Conference Proceedings*, vol. 1297, pp. 135–338 (American Institute of Physics, 2010). https://doi.org/10.1063/1.3518900.
13. K. Binder, Finite size scaling analysis of Ising model block distribution functions. *Zeitschrift für Physik B Condensed Matter* 43(2), 119 https://doi.org/10.1007/BF01293604 (1981).
14. R. Gebarowski, Monte Carlo simulations of the Ising model on a square lattice with random gaussian interactions. *Czasopismo Techniczne*. https://doi.org/10.4467/2353737XCT.14.312.3400 (2014).
15. A. Sonsin, M. Cortes, D. Nunes, J. Gomes, and R. Costa, Computational analysis of 3d Ising model using metropolis algorithms. *J. Phys. Conf. Ser.* 630, 012057 https://doi.org/10.1088/1742-6596/630/1/012057 (2015).
16. J. Selinger, *Introduction to the Theory of Soft Matter, Soft and Biological Matter* (Springer, Switzerland, 2016).
17. G. Shirane, Neutron scattering studies of structural phase transitions at Brookhaven. *Rev. Mod. Phys.* 46(3), 437 (1974).
18. S. Callori, S. Hu, J. Bertinshaw, Z. Yue, S. Danilkin, X. Wang, V. Nagarajan, F. Klose, J. Seidel, and C. Ulrich, Strain-induced magnetic phase transition in srcoo 3-δ thin films. *Phys. Rev. B* 91(14), 140405 (2015).
19. T. Nishio, M. Yamamoto, T. Ohkochi, D. Nanasawa, A. Foggiatto, and M. Kotsugi, High-throughput analysis of magnetic phase transition by combining table-top sputtering, photoemission electron microscopy, and landau theory. *Sci. Technol. Adv. Mater. Methods* 2(1), 345 (2022).
20. S. Kaul, On the ferromagnetic–paramagnetic phase transition in amorphous iron-rich fe100-xzrx (x = 8, 9, 10) alloys. *J. Phys. F Met. Phys.* 18(9), 2089 https://doi.org/10.1088/0305-4608/18/9/026 (1988).
21. H. Yamauchi, H. Onodera, and H. Yamamoto, Anomalous critical behavior of amorphous $Fe_{100-x}Zr_x$ ferromagnets (x = 8 and 10). *J. Phys. Soc. Jpn.* 53(2), 747 https://doi.org/10.1143/JPSJ.53.747 (1984).
22. L. Schoop, M. Hirschberger, J. Tao, C. Felser, N.P. Ong, and R.J. Cava, Paramagnetic to ferromagnetic phase transition in lightly Fe-doped Cr_2B. *Phys. Rev. B* 89(22), 224417 https://doi.org/10.1103/PhysRevB.89.224417 (2014).
23. C.-W. Liu, A. Polkovnikov, and A.W. Sandvik, Dynamic scaling at classical phase transitions approached through nonequilibrium quenching. *Phys. Rev. B* 89(5), 054307 (2014).
24. Z.E. Eğer and P. Acar, Uncertainty quantification of phase transitions in magnetic materials lattices. *Appl. Phys. Lett.* 124(2), 66 (2024).
25. Z.E. Eger and P. Acar, Eliminating magnetic phase transitions with microstructural optimization in 2d lattices, in *AIAA SCITECH 2024 Forum*, p. 0030 (2024).
26. P. Acar and V. Sundararaghavan, Do epistemic uncertainties allow for replacing microstructural experiments with reconstruction algorithms? *AIAA J.* 57(3), 1078 https://doi.org/10.2514/1.J057488 (2019).
27. P. Acar and V. Sundararaghavan, A Markov random field approach for modeling spatio-temporal evolution of microstructures. *Model. Simul. Mater. Sci. Eng.* 24(7), 075005 https://doi.org/10.1088/0965-0393/24/7/075005 (2016).
28. M.M. Hasan, A. Senthilnathan, and P. Acar, Uncertainty dominated phase transitions of 2D magnetic materials, in *AIAA SCITECH 2022 Forum*, p. 0504 (2022).
29. R.P. Feynman, R.B. Leighton, and M. Sands, The Feynman lectures on physics; vol. i. *Am. J. Phys.* 33(9), 750 https://doi.org/10.1119/1.1972241 (1965).
30. T. Kennedy, *Math 541: Introduction to Mathematical Physics Lecture Notes* (University of Arizona, 2008).